ACS APPLIED MATERIALS & INTERFACES

Letter

www.acsami.org

Oriented Film Growth of $Ba_{1-x}Sr_xTiO_3$ Dielectrics on Glass Substrates Using 2D Nanosheet Seed Layer

Chulho Jung, Tsuyoshi Ohnishi, Minoru Osada,* Kazunori Takada, and Takayoshi Sasaki*

International Center for Materials Nanoarchitectonics (MANA), Global Research Center for Environment and Energy Based on Nanomaterials Science (GREEN), and Environmental and Energy Materials Division, National Institute for Materials Science, 1-1 Namiki, Tsukuba 305-0044, Japan

Supporting Information

ABSTRACT: An approach to fabricate $Ba_{0.5}Sr_{0.5}TiO_3$ (BST) films with a preferred orientation on a glass substrate by pulsed laser deposition was developed. To ensure a preferred crystallographic orientation, we utilized a molecularly thin $Ca_2Nb_3O_{10}$ perovskite nanosheet as a seed layer and successfully fabricated BST films with a nearly perfect (100)-axis orientation. The 100 nm films after annealing at 450 °C in air showed a good dielectric performance (ε_r > 400), which was comparable to the ε_r value of epitaxially grown films with the same thickness. These results indicate that the nanosheet seed layer plays a crucial role in controlled film growth, realizing a nearly intrinsic performance of BST.

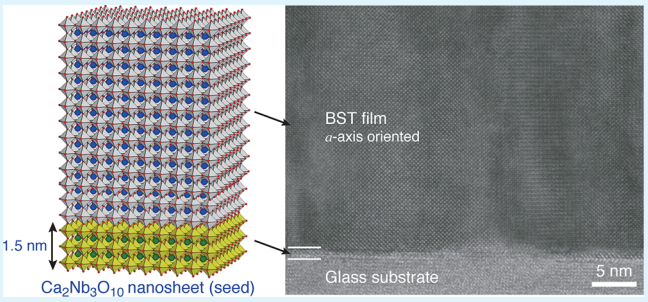

KEYWORDS: *nanosheet, seed layer, $Ba_{1-x}Sr_xTiO_3$, thin-film growth, dielectrics*

Crystallographic orientation control of thin films is critically important when the films are used for characterizing or optimizing anisotropic physical properties of materials.[1] Such an issue is clearly exposed in perovskite oxides such as $(Ba,Sr)TiO_3$, $PbTiO_3$, $SrBi_2Ta_2O_9$, and $Bi_4Ti_3O_{12}$.[1−5] In these perovskite oxides, the dielectricity/ferroelectricity is a directional property in which excellent properties occur only in the direction of the polar axis. Therefore, to fully utilize the remarkable anisotropy-dependent properties of perovskite oxides, it is necessary to carefully control the microstructural orientation during processing. Perovskite thin films with a preferred orientation exhibited unique and sometimes improved permittivity/polarization, in comparison to those of randomly oriented films.

The orientation control has been achieved by modifying the template surface with single-crystal substrates. In previous studies on simple perovskite oxides such as $(Ba,Sr)TiO_3$ and $PbTiO_3$, single-crystal substrates such as $LaAlO_3$, MgO, and $SrTiO_3$ were usually utilized because their precisely controlled lattice matching with a good chemical compatibility enables oriented growth of high-quality thin films.[1,5−9] Can analogous "template" approaches be used to grow uniaxial-oriented films on cheap and conventional substrates such as a glass, Si, metals, and plastics? This remains an unresolved and challenging issue in the practical applications such as MEMS and Si electronics.

We address this issue by introducing a new seed-layer technique; two-dimensional (2D) oxide nanosheets are used to promote oriented crystal growth on surfaces. The nanosheets are obtained by delaminating layered host compounds into elementary layers with a thickness of 1−2 nm via a soft-chemical process.[10,11] The obtained single sheets inherit the well-ordered 2D crystalline lattice of the original host materials, providing 2D crystal surfaces as a trigger for controlled nucleation of crystals. Recently, we have demonstrated the oriented film growth of some important oxides of TiO_2, $SrTiO_3$, and ZnO using a seed layer of oxide nanosheets;[12−14] $Ca_2Nb_3O_{10}$ is applied for the former two cases, whereas MnO_2 and $Cs_4W_{11}O_{36}$ are used for the latter. In the perovskite $SrTiO_3$ case, we utilized the sol−gel process for the film growth of $SrTiO_3$.[12] However, the obtained film quality was still far from satisfactory because of the essential difficulty in controlling the crystallization process by the sol−gel method. Physical vapor deposition techniques may provide a suitable clue for preparing high-quality perovskite films, being similar to those using lattice-matched single-crystal substrates. Furthermore, physical properties of nanosheet-seed films have not yet been fully explored; a majority of research was limited to the fabrication and characterization of oriented films. Exploring the dielectric property of the oriented films fabricated by the seed-layer technique is of particularly importance as it might shed new insights into dielectric properties of nanosheet-seed films and provide a prospective for future applications.

In this study, we report the orientation-controlled deposition of highly crystalline $Ba_{1-x}Sr_xTiO_3$ (BST) dielectric thin films by pulsed laser deposition (PLD), whereby nearly perfect *a*-axis orientation was successfully achieved on a glass substrate using

Received: March 7, 2013
Accepted: May 21, 2013
Published: May 31, 2013

   dx.doi.org/10.1021/am400849z | ACS Appl. Mater. Interfaces 2013, 5, 4592−4596

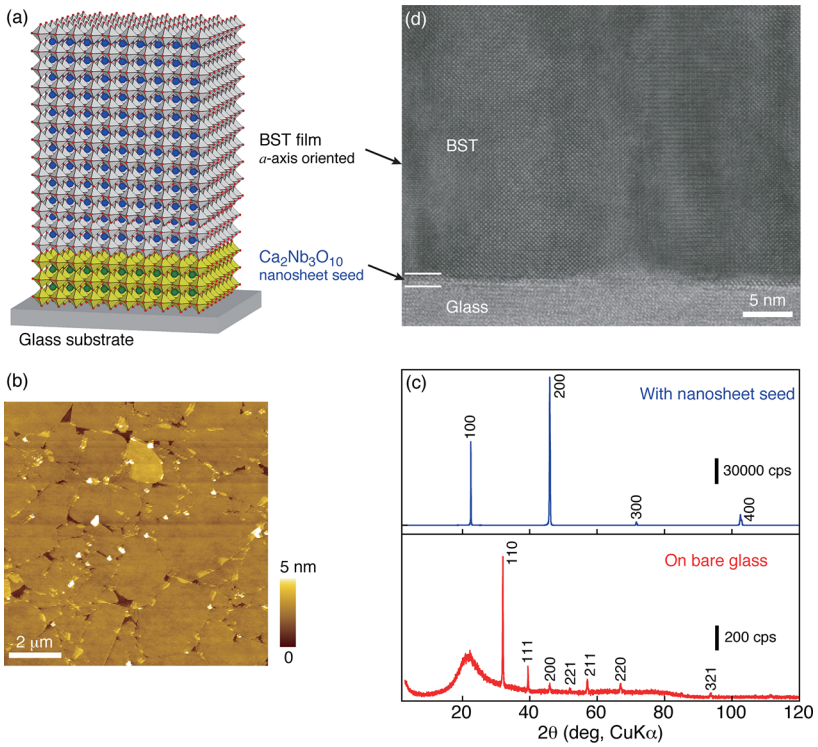

Figure 1. (a) Schematic illustration for oriented film growth of BST on glass substrate using a $Ca_2Nb_3O_{10}$ nanosheet seed layer. (b) AFM image of the monolayer film of $Ca_2Nb_3O_{10}$ nanosheets deposited on a glass substrate. (c) XRD patterns of BST films deposited on glass substrates with and without a nanosheet seed layer. A broad hump centered at 25° in 2θ is attributable to a halo from the glass substrate. (d) Cross-sectional HRTEM image of BST film with a nanosheet seed layer.

a unilamellar $Ca_2Nb_3O_{10}$ nanosheet as a seed layer. The resulting films showed a high dielectric response (ε_r > 400), which was comparable to the ε_r value of epitaxially grown films with the same thickness.

Figure 1a presents our nanosheet-seed approach for fabricating BST dielectric films with (100)-axis orientation on a glass substrate; fabrication of a monolayer film of nanosheets as the first step and PLD deposition of BST films as the second step. Perovskite $Ca_2Nb_3O_{10}$ nanosheet with a 2D square atomic arrangement was used as a source for the seed layer for BST. In this study, we choose a highly Sr-doped composition ($Ba_{0.5}Sr_{0.5}TiO_3$) by considering the in-plane lattice matching between BST crystal (a = 0.395 nm)[15] and $Ca_2Nb_3O_{10}$ nanosheet (a = 0.386 nm);[16] higher Sr content causes the shrinkage of the lattice parameters,[6] inducing a better lattice matching.

A unilamellar $Ca_2Nb_3O_{10}$ nanosheet was prepared by delaminating a layered perovskite $KCa_2Nb_3O_{10}$ according to previously described procedures.[16] A VIOSIL glass (Shin-Etsu Chemical Ltd.) was used as a substrate. This glass substrate has a high heat-resistant property; a strain point is higher than 950 °C, which is suitable for the use for PLD at high temperature (see the Supporting Information). A monolayer film of $Ca_2Nb_3O_{10}$ nanosheets was transferred onto a glass substrate by the Langmuir−Blodgett (LB) method, as described in detail elsewhere.[17,18] This LB deposition of $Ca_2Nb_3O_{10}$ nanosheets led to the formation of ultimately thin seed layers on amorphous glass substrates at room temperature. The surface morphology was studied by atomic force microscopy (AFM). Figure 1b depicts a typical AFM image of a monolayer film of $Ca_2Nb_3O_{10}$ nanosheets on a glass substrate. Individual nanosheets with an average lateral dimension of 1−5 μm were clearly resolved, confirming substantial monolayer coverage of neatly packed nanosheets. The surface of the film was mostly flat, except for small gaps and overlaps. The root-mean-square surface roughness was estimated to be 0.8 nm, being almost comparable to single-crystal substrates.

BST films were deposited on the glass substrates with the $Ca_2Nb_3O_{10}$ nanosheet seed layer by PLD, employing a KrF excimer laser (λ = 248 nm). Sintered $Ba_{0.5}Sr_{0.5}TiO_3$ pellets were used as PLD targets. The film deposition was performed under optimized conditions (temperature: 800 °C, oxygen partial pressure: 8 × 10^{-5} Pa, laser energy density: 0.22 J cm^{-2}, repetition frequency: 20 Hz). Sufficient preablation was performed before deposition until the target surface reached a steady state for each combination of parameters.[19,20] The film thickness was fixed at ∼100 nm by controlling the deposition time.

Figure 1c compares X-ray diffraction (XRD) patterns of BST films deposited on glass substrates with and without the $Ca_2Nb_3O_{10}$ nanosheet seed layer. In the film deposited on the bare glass substrate, several diffraction peaks with indices of 110, 111, 200, 221, 211, 220, and 321 were observed, which is characteristic of randomly orientated polycrystalline sample. On the other hand, the film growth on the nanosheet seed layer gave strong and sharp h00 diffraction peaks. The film prepared on the nanosheet seed layer showed higher crystallinity than the control sample as revealed by the narrower linewidths of the diffraction peaks. Regarding the 200 reflection, a full width at half-maximum (fwhm) of 0.18 and 0.33° was obtained for BST films with and without the nanosheet seed layer, respectively. Therefore, the crystal sizes (t) for these two films were estimated to be 48 and 27 nm using Scherrer's equation

dx.doi.org/10.1021/am400849z | ACS Appl. Mater. Interfaces 2013, 5, 4592−4596

$$t = \frac{K\lambda}{\beta \cos\theta}$$

where K is Scherrer's constant (0.9), λ is the wavelength of radiation (0.15404 nm), and β is the fwhm of the peak (in radians 2θ) located at angle θ (2θ = 45.93°). These results clearly indicate that the $Ca_2Nb_3O_{10}$ nanosheets can promote oriented growth of BST, giving a dramatic difference in film quality and crystallographic orientation. The enhancement in crystallinity is an additional advantage of the nanosheet seed layers. The *a*-axis lattice parameter of the obtained BST film was refined to be 0.3965(2) nm, which was slightly larger than that of BST bulk ceramics (0.395 nm with cubic symmetry).[15] This is presumably due to the lattice mismatch between BST and $Ca_2Nb_3O_{10}$ nanosheet.[15,16,21]

Cross-sectional high-resolution transmission electron microscopy (HRTEM) observation was carried out to visualize the film texture at the nanoscopic level (Figure 1d). TEM image clearly revealed uniform film formation with a highly oriented structure. At the film/substrate interface, a 1−2 nm-thick seed layer was clearly resolved, again indicating that the 2D surface of $Ca_2Nb_3O_{10}$ nanosheets can promote the well-ordered film growth. A clear benefit of our approach is the experimental realization of an atomically sharp, clean interface between the film and the substrate. In perovskite thin films, the formation of the interfacial dead layers is a longstanding problem, which causes the degradation of dielectric/ferroelectric properites.[22] In our case, there was no detectable interdiffusion at the interface. It is also noteworthy that $Ca_2Nb_3O_{10}$ nanosheet possesses high-*k* permittivity (ε_r = 210) even in the ultrathin form.[18] In our preliminary investigations, we found a robust thermal stability (>700 °C) in monolayer films (see the Supporting Information, Figure S1); a stable high-*k* dielectric response (ε_r > 100) in the nanosheet films persisted at >700 °C. Therefore, our nanosheet-seed approach can create a dead-layer-free BST film deposited on the glass substrate by engineering the high-*k* seed interface at the atomic scale, which may realize the full potential of high-*k* perovskites.

We investigated dielectric properties of the fabricated BST films. The as-deposited BST films were in slightly reduced state because of the PLD conditions employed. Oxygen vacancy may be involved, giving rise to electrical conductivity of the film. Prior to dielectric measurements, the as-deposited films were postannealed in air at 450 °C for 1−10 h to obtain fully oxidized films with an insulating nature. Figure 2 shows the variation of the optical transmittance and *a*-axis parameter as a function of annealing time. Here we monitored the optical transmittance at 2 μm to characterize the conducting behavior of the film since free carriers associated with oxygen vacancies show a broad feature centered at this wavelength.[23] The transmittance of the as-deposited films was ~44%, which increased to ~65% by annealing for 1 h. Prolonged annealing did not cause further change in the transmittance. The lattice parameter showed a similar trend; the *a* parameter expanded by ca. 0.0005 nm in 2 h and stayed substantially constant by further annealing. This close correlation between the transmittance and lattice constant suggests that oxygen deficiency in the as-deposited film was recovered by annealing for 1−2 h. In this context, a relatively large variation of the lattice parameter was observed for 2 h. This might be related to the lattice relaxation during the oxidation process. Preliminary electrical conductivity measurements confirmed that the film became highly insulating (<1×10^{-7} A cm^{-2}) by the annealing process, further supporting the substantial oxidation. In this process, the orientation and crystallinity of the films remained practically unchanged.

The resulting films were found to exhibit remarkable dielectric properties. The dielectric properties of films were measured using planar interdigital electrodes (see the Supporting Information, Figure S2).[24−26] Details for experimental procedure is described in the Supporting Information. Figure 3a shows the frequency dependence of the relative

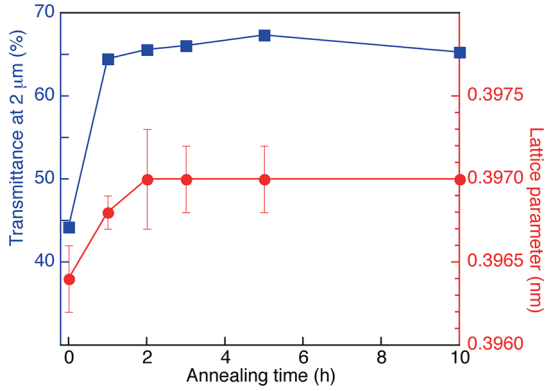

Figure 2. Effects of annealing on the optical transmittance at 2 μm (square) and *a*-axis parameter (circles) for BST films deposited on glass substrates with a nanosheet seed layer.

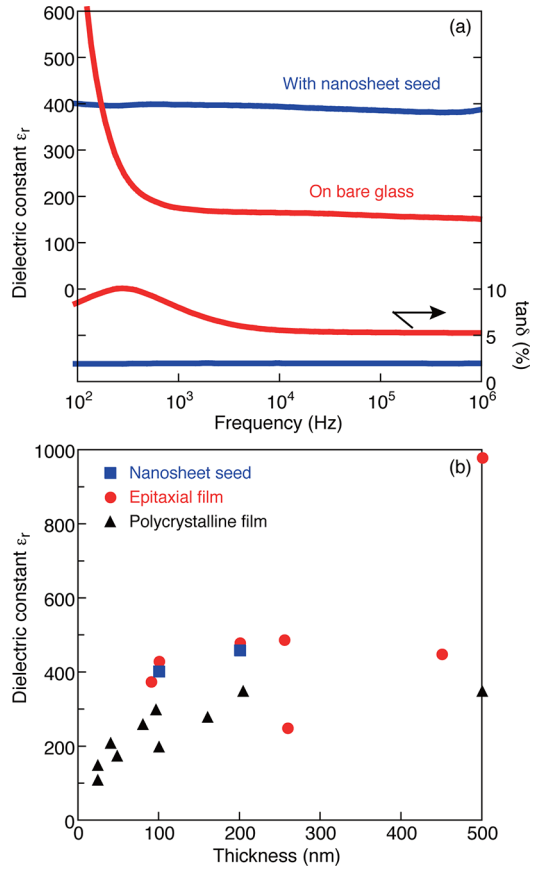

Figure 3. (a) Dielectric constant ε_r and dielectric loss tan δ of BST films deposited on glass substrates with and without a nanosheet seed layer. (b) Thickness dependence of the maximum ε_r value for BST films with different epitaxial qualities.

dx.doi.org/10.1021/am400849z | ACS Appl. Mater. Interfaces 2013, 5, 4592−4596

dielectric constant (ε_r) for BST films grown on the glass substrates with and without the nanosheet seed layer. Figure 3b summarizes the thickness dependence of the maximum ε_r value for BST films with different epitaxial qualities. Complementary result obtained from 200-nm thick film with the nanosheet seed layer is also included in this figure. The highly oriented BST with the nanosheet seed layer showed a high dielectric response (ε_r = 370−420), which was almost comparable to the ε_r value of epitaxially grown films with the same thickness.[6−9,27] The ε_r values also exhibited a rather flat frequency dispersion within 10% in the regime of 1 kHz to 1 MHz where the dielectric loss tanδ was around ∼3%. In contrast, the BST film without the nanosheet seed layer had greatly deteriorated properties (ε_r = 146−168, tan $\delta \approx$ 5%).

These differences in ε_r and tan δ for the films are ascribable to their sharp differences in film architecture and orientation. The higher ε_r for the BST films on the nanosheet compared to that on the bare glass can be basically due to both higher crystallinity and larger grain size of the films. The film grown without the nanosheet seed layer was randomly orientated and poorly crystalline with a much smaller grain size, deteriorating its dielectric performance. This behavior is consistent with previous reports, which indicate a reduced dielectric performance ($\varepsilon_r \leq 300$) for polycrystalline films.[28,29]

The origin for the similar dielectric response between the films on nanosheet with one-axis orientation and the epitaxial films is not clearly understood. Although the in-plane random nature in our BST films may influence the dielectric response, there might be additional factors such as strain and interface effects. The BST films deposited at higher temperatures are more stretched in the in-plane direction due to the mismatch of thermal expansion coefficients between the film and the substrate. In such a case, a large dielectric anisotropy exists in the films with better in-plane dielectric properties (dielectric constant, tunability) than those along the out-of-plane direction. We indeed found a large tunability (∼23% at 100 kV/cm) of BST films on the nanosheet (see the Supporting Information, Figure S3). In our case, however, BST films on the nanosheet is under compressive stress, and the in-plane dielectric constant should be smaller than the out-of-plane dielectric constant because the in-plane compressive stress can reduce the in-plane dielectric constant.

Another possible origin that supports the obtained results is associated with the different response of the interfacial dead layer effect.[22] In our measurements with the coplanar capacitance configuration, the thickness dependence of ε_r appeared to be analogous to previous reports on epitaxial BST films with the metal/insulator/metal (MIM) capacitor structure. However, these two cases are based on different mechanisms. In the MIM capacitor structure, the reduction in ε_r in BST thin films could be explained by the existence of the interfacial low-k layer (the so-called "dead layer") between the BST film and the substrate; the influence of the dead layer with low ε_r becomes significant, causing a reduced total capacitance. In our case with the coplanar capacitance structure, however, the thickness effect cannot be understood by such dead layer model, because the capacitance contribution of the dead layer to the total capacitance of the interdigital capacitor is negligible according to the partial capacitance model.[24,30] Thus, the interfacial effect is well-suppressed in the in-plane measurement geometry, and the impact of the interfacial low-k layer on the measured ε_r value is not obvious for the BST films with the coplanar structure, giving rise to high dielectric permittivity. In our case, the increase in ε_r with increasing the film thickness is possibly due to strain relaxation. Although further investigations are necessary for full understanding the influence of the nanosheet seed layer on dielectric properties, our work opens up new possibility of interface engineering for film architectures with enhanced dielectric properties.

In summary, we successfully fabricated highly oriented BST dielectric thin films onto a glass substrate, promoted by $Ca_2Nb_3O_{10}$ nanosheet as a seed layer. A simple, inexpensive process, by LB deposition using atomically flat nanosheets, led to the formation of ultimately thin seed layers on amorphous glass substrates at room temperature. Such nanosheet seed layers can promote oriented growth of BST films with a nearly perfect a-axis orientation. The resulting BST films realized a nearly intrinsic performance (ε_r = 370−420) comparable to the epitaxially grown films. Although this study has focused on the film fabrication on glass substrates, our nanosheet seed approach is not limited to the glass substrate. Such a capability of the template surface modification is critically important in the fields of ferroelectrics/piezoelectrics.

■ ASSOCIATED CONTENT

Ⓢ Supporting Information

Details of nanosheet synthesis, LB deposition of the nanosheet seed layer, PLD of BST films, sample characterization, thermal stability of nanosheet-coated glass substrate, and dielectric measurements. This material is available free of charge via the Internet at http://pubs.acs.org.

■ AUTHOR INFORMATION

Corresponding Author

*E-mail: sasaki.takayoshi@nims.go.jp (T.S.); osada.minoru@nims.go.jp (M.O.).

Funding

The authors declare no competing financial interest.

Notes

The authors declare no competing financial interest.

■ ACKNOWLEDGMENTS

This work was supported by the CREST program of the Japan Science and Technology Agency (JST) and World Premier International Research Center (WPI) Initiative on Materials Nanoarchitectonics, MEXT, Japan.

■ REFERENCES

(1) Schlom, D. G.; Chen, L. Q.; Pan, X.; Schmehl, A.; Zurbuchen, M. A. *J. Am. Ceram. Soc.* **2008**, *91*, 2429−2454.
(2) Lee, H. N.; Hesse, D.; Zakharov, N.; Gösele, U. *Science* **2002**, *296*, 2006−2009.
(3) Watanabe, T.; Funakubo, H.; Saito, K.; Suzuki, T.; Fujimoto, M.; Osada, M.; Noguchi, Y.; Miyayama, M. *Appl. Phys. Lett.* **2002**, *81*, 1660−1662.
(4) Watanabe, T.; Funakubo, H. *J. Appl. Phys.* **2006**, *100*, 051602.
(5) Vrejoiu, I.; Alexe, M.; Hesse, D.; Gösele, U. *Adv. Funct. Mater.* **2008**, *18*, 3892−3906.
(6) Chang, W.; Gilmore, C. M.; Kim, W. J.; Pond, J. M.; Kirchoefer, S. W.; Qadri, S. B.; Chirsey, D. B.; Horwitz, J. S. *J. Appl. Phys.* **2000**, *87*, 3044−3049.
(7) Carlson, C. M.; Rivkin, T. V.; Parilla, P. A.; Perkins, J. D.; Ginley, D. S.; Kozyrev, A. B.; Oshadchy, V. N.; Pavlov, A. S. *Appl. Phys. Lett.* **2000**, *76*, 1920−1922.
(8) Moon, S. E.; Kim, E. K.; Kwak, M. H.; Ryu, H. C.; Kim, Y. T.; Kang, K. Y.; Lee, S. J.; Kim, W. J. *Appl. Phys. Lett.* **2003**, *83*, 2166−2168.

(9) Chang, K. S.; Aronova, M.; Famodu, O.; Takeuchi, I.; Lofland, S. E.; Hattrick-Simpers, J.; Chang, H. *Appl. Phys. Lett.* **2001**, *79*, 4411−4413.
(10) Sasaki, T.; Watanabe, M. *J. Am. Chem. Soc.* **1998**, *120*, 4682−4689.
(11) Ma, R.; Sasaki, T. *Adv. Mater.* **2010**, *22*, 5082−5104.
(12) Shibata, T.; Fukuda, K.; Ebina, Y.; Kogure, T.; Sasaki, T. *Adv. Mater.* **2008**, *20*, 231−235.
(13) Shibata, T.; Ohnishi, T.; Sakaguchi, I.; Osada, M.; Takada, K.; Kogure, T.; Sasaki, T. *J. Phys. Chem. C* **2009**, *113*, 19096−19101.
(14) Shibata, T.; Ebina, Y.; Ohnishi, T.; Takada, K.; Kogure, T.; Sasaki, T. *Cryst. Growth Des.* **2010**, *10*, 3787−3793.
(15) McQuarrie, M. *J. Am. Ceram. Soc.* **1955**, *38*, 444−449.
(16) Ebina, Y.; Sasaki, T.; Watanabe, M. *Solid State Ionics* **2002**, *151*, 177−182.
(17) Akatsuka, K.; Haga, M.; Ebina, Y.; Osada, M.; Fukuda, K.; Sasaki, T. *ACS Nano* **2009**, *3*, 1097−1106.
(18) Osada, M.; Akatsuka, K.; Ebina, Y.; Funakubo, H.; Ono, K.; Takada, K.; Sasaki, T. *ACS Nano* **2010**, *4*, 5225−5232.
(19) Ohnishi, T.; Lippmaa, M.; Yamamoto, T.; Meguro, S.; Koinuma, H. *Appl. Phys. Lett.* **2005**, *87*, 241919.
(20) Ohnishi, T.; Shibuya, K.; Yamamoto, T.; Lippmaa, M. *J. Appl. Phys.* **2008**, *103*, 103703.
(21) Alldredge, L. M. B.; Chang, W.; Qadri, S. B.; Kirchoefer, S. W.; Pond, J. M. *Appl. Phys. Lett.* **2007**, *90*, 212901.
(22) Stengel, M.; Spaldin, N. A. *Nature* **2006**, *443*, 679−682.
(23) Lee, C.; Destry, J.; Brebner, J. L. *Phys. Rev. B* **1975**, *11*, 2299−2310.
(24) Song, S. N.; Zhai, J. W.; Gao, L. N.; Yao, X.; Hung, T. F.; Xu, Z. K. *J. Appl. Phys.* **2008**, *104*, 096107.
(25) Zhu, X. H.; Guigues, B.; Defaÿ, E.; Dubarry, C.; Aïd, M. *J. Appl. Phys.* **2009**, *106*, 024109.
(26) Gevorgian, S. S.; Martinsson, T.; Linner, P. L. J.; Kollberg, E. L. *IEEE Trans. Microwave Theory Tech.* **1996**, *44*, 896−904.
(27) Kim, W. J.; Chang, W.; Qadri, S. B.; Pond, J. M.; Kirchoefer, S. W.; Chrisey, D. B.; Horwitz, J. S. *Appl. Phys. Lett.* **2000**, *76*, 1185−1187.
(28) Basceri, C.; Streiffer, S. K.; Kingon, A. I.; Waser, R. *J. Appl. Phys.* **1997**, *82*, 2497−2504.
(29) Kim, T. S.; Kim, C. H.; Oh, M. H. *J. Appl. Phys.* **1994**, *75*, 7998−8003.
(30) Zhou, X. Y.; Wang, D. Y.; Zheng, R. K.; Tian, H. Y.; Qi, J. Q.; Chan, H. L. W.; Choy, C. L.; Wang, Y. *Appl. Phys. Lett.* **2007**, *90*, 132902.